arXiv:1408.0558v1 [physics.flu-dyn] 4 Aug 2014

Collective Dynamics of Interacting Particles in Unsteady Flows

Maryam Abedi and Mir Abbas Jalali*

Computational Mechanics Laboratory,

Department of Mechanical Engineering,

Sharif University of Technology, Azadi Avenue,

P.O. Box: 11155-9567, Tehran, Iran

Abstract

We use the Fokker-Planck equation and its moment equations to study the collective behavior of interacting particles in unsteady one-dimensional flows. Particles interact according to a long-range attractive and a short-range repulsive potential field known as Morse potential. We assume Stokesian drag force between particles and their carrier fluid, and find analytic single-peaked traveling solutions for the spatial density of particles in the catastrophic phase. In steady flow conditions the streaming velocity of particles is identical to their carrier fluid, but we show that particle streaming is asynchronous with an unsteady carrier fluid. Using linear perturbation analysis, the stability of traveling solutions is investigated in unsteady conditions. It is shown that the resulting dispersion relation is an integral equation of the Fredholm type, and yields two general families of stable modes: singular modes whose eigenvalues form a continuous spectrum, and a finite number of discrete global modes. Depending on the value of drag coefficient, stable modes can be over-damped, critically damped, or decaying oscillatory waves. The results of linear perturbation analysis are confirmed through the numerical solution of the fully nonlinear Fokker-Planck equation.

* mjalali@sharif.edu

I. INTRODUCTION

Collective motion of interacting particles is observed in various natural systems, from large-scale schools of fishes [1] and the flock of birds [2] to small-scale aggregation of red blood cells (RBC) [3] and bacterial colonies [4]. To elucidate the mechanisms leading to formation of this self organized patterns, several particle based [5, 6], continuum kinetic [7] and hydrodynamic models [8] have been developed. In these systems, the population organization is affected by the influence zone [9], leadership [10], geometrical constraints [9] and also by environmental factors like the drag force [6] and random noise in particle velocities [11].

The organized movement of particles becomes more complex if they move in a transient carrier fluid. For instance, the collaborative flock of birds in windy conditions, and the swim of fishes in rivers or along oceanic currents is poorly understood, and we know a little about the stability of their group behavior in time-varying flow fields. The collective dynamics of RBCs in blood vessels is also expected to correlate with the chaotic nature of the heart beat [12] and its influence on the blood stream. Moreover, micro-organisms produce different collective behavior in the presence of turbulence [13], vortices [14] and shear flow [15]. Hydrodynamic models of self-propelled, non-interacting particles in an incompressible fluid show that a concentrated population of swimming bacteria in an incompressible fluid exhibits spatiotemporal patterns [16, 17]. Other works in the literature have only addressed the swarm of interacting particles in the absence of inertial effects and when the carrier fluid has a constant velocity [18–20]. It is therefore important to understand how particle–particle interactions and the drag force of an unsteady carrier fluid can collaborate to develop patterns in the spatial distribution of particles, and whether such patterns can remain stable.

The flock/swarm pattern depends on the interaction between particles. A widely used interaction model is the Morse potential, which can produce various collective behaviors, including localized flocks and vortex solutions, in one- and two-dimensional systems [6, 21, 22]. The parameters of the Morse potential control the phase, catastrophic or H-stable, and morphology of self-organized systems. A system consisting of N interacting particles and with the total potential energy U, is in H-stable phase if the quantity U/N has a lower negative bound, and the system does not collapse in the limit of $N \to \infty$. In such conditions the swarm size typically increases with the number of particles. Non-H-stable systems with

particles collapsing into a dense body are called catastrophic [23]. Here, we adopt the Morse potential and study the dynamics of colonies of particles in one-dimensional flows. The Fokker-Planck equation is used to trace the dynamics of particles as they sense the unsteady motion of carrier fluid through Stokesian drag. The response of flocking particles to disturbances in the density and streaming velocity, and the effect of drag coefficient on stability characteristics, are investigated for the first time.

The paper is organized as follows. In section II, we introduce our model and derive the kinetic and hydrodynamic equations using the motion equations of individual particles. In section III, we explain numerical algorithms that have been used to solve the Fokker-Planck equation. The collective dynamics of particles in steady flows is studied in section IV and exact analytical solutions are found for catastrophic swarms of particles. In section V, we present analytical solutions for the streaming of particles in unsteady flow conditions, and perturb the continuity and momentum equations to investigate the linear stability of these time-varying collective motions. The results of the linear perturbation analysis are verified using numerical solutions of the Fokker-Planck equation. Our concluding remarks are presented in section VI.

II. KINETIC AND HYDRODYNAMIC EQUATIONS

We assume that particles move in a Newtonian fluid and the drag force exerted on the ith particle, with the position x_i and velocity v_i, is computed from $-\beta(v_i - u_{\rm f})$. Here $u_{\rm f}(x,t)$ is the streaming velocity of the carrier fluid, and β is the Stokesian drag coefficient. The equations of motion for the ith particle read

$$\dot{x}_i = v_i, \quad \dot{v}_i = -\frac{1}{N}\sum_{j=1}^{N} \partial_{x_i}\Phi(r_{ij}) - \beta(v_i - u_{\rm f}), \quad i = 1, 2, \ldots, N, \tag{1}$$

with $r_{ij} = |x_i - x_j|$ and $\partial_{x_i} = \partial/\partial x_i$. Φ is the two-body Morse potential defined as

$$\Phi(r_{ij}) = c_1 e^{-r_{ij}/d_1} - c_2 e^{r_{ij}/d_2}, \tag{2}$$

which has been widely used to describe red blood cell aggregation [24] and the swarm of animals [25]. The positive parameters d_2 and d_1 are, respectively, the attraction and repulsion length scales, and $c_1 > 0$ and $c_2 > 0$ are force magnitudes. Long-range attractive, and short-range repulsive forces are obtained by setting $d_1/d_2 < 1$ and $c_1/c_2 > 1$.

Let $f^{(N)}\left(\{x_i\},\{v_i\},t\right)$ $(i=1,2,\ldots,N)$ be the N-particle probability distribution function (DF) at time t. The probability of finding the ith particle at the position x_i with the velocity v_i within an infinitesimal phase space volume $\mathrm{d}\mathcal{V}=\Pi_{i=1}^{N}\mathrm{d}x_i\mathrm{d}v_i$ is $f^{(N)}\mathrm{d}\mathcal{V}$. Since the mass of the entire N-particle system is conserved, the temporal evolution of $f^{(N)}$ is governed by Liouville's equation [26]:

$$\frac{\partial f^{(N)}}{\partial t}+\sum_{i=1}^{N}\left[\partial_{x_i}\left(\dot{x_i}f^{(N)}\right)+\partial_{v_i}\left(\dot{v_i}f^{(N)}\right)\right]=0, \tag{3}$$

The one-particle DF is obtained by integrating $f^{(N)}$ as

$$f^{(1)}(x_1,v_1,t)=\int_{\mathcal{V}_1}f^{(N)}(x_1,x_2,\ldots,x_N,v_1,v_2,\ldots,v_N,t)\,\mathrm{d}\mathcal{V}_1, \tag{4}$$

where $\mathcal{V}_1$ is an $(N-2)$ dimensional subspace of $\mathcal{V}$. The evolutionary equation of $f^{(1)}$ can therefore be obtained through integrating equation (3) as

$$\frac{\partial f^{(1)}}{\partial t}+\int_{\mathcal{V}_1}\left[\partial_{x_1}\left(\dot{x_1}f^{(N)}\right)+\partial_{v_1}\left(\dot{v_1}f^{(N)}\right)\right]\,\mathrm{d}\mathcal{V}_1=0. \tag{5}$$

Substituting from (1) into (5) gives

$$\frac{\partial f^{(1)}}{\partial t}+v_1\frac{\partial f^{(1)}}{\partial x_1}+\frac{\partial}{\partial v_1}\left[-\beta(v_1-u_{\mathrm{f}})f^{(1)}\right]+\mathcal{A}=0, \tag{6}$$

with

$$\mathcal{A}=-\frac{1}{N}\sum_{j=2}^{N}\int_{\mathcal{V}_1}\partial_{v_1}\left[f^{(N)}\partial_{x_1}\Phi(r_{1j})\right]\,\mathrm{d}\mathcal{V}_1. \tag{7}$$

All integrals within the summation are identical: they are evaluated over $(N-2)$ dimensional subspaces of $\mathcal{V}$, and there are $N-1$ of such integrals/subspaces. One thus finds

$$\mathcal{A}=-\frac{N-1}{N}\int_{\mathcal{V}_1}\partial_{v_1}\left[f^{(N)}\partial_{x_1}\Phi(r_{12})\right]\,\mathrm{d}\mathcal{V}_1=-\frac{N-1}{N}\int\partial_{v_1}\left[f^{(2)}\partial_{x_1}\Phi(r_{12})\right]\,\mathrm{d}x_2\mathrm{d}v_2, \tag{8}$$

where the two-particle DF $f^{(2)}(x_1,v_1,x_2,v_2,t)$ is obtained by integrating $f^{(N)}$ over an $(N-4)$ dimensional subspace of $\mathcal{V}$. In a system with long-range interactions, when the relaxation time becomes sufficiently large in the thermodynamic limit $N\to\infty$, two-particle correlations are neglected and one can work with the separable form [26]

$$f^{(2)}(x_1,x_2,v_1,v_2,t)=f^{(1)}(x_1,v_1,t)f^{(1)}(x_2,v_2,t). \tag{9}$$

Substituting from equation (9) into (8) leads to

$$\mathcal{A}=-\frac{N-1}{N}\int\frac{\partial}{\partial v_1}\left[f^{(1)}(x_1,v_1,t)f^{(1)}(x_2,v_2,t)\partial_{x_1}\Phi(r_{12})\right]\,\mathrm{d}x_2\mathrm{d}v_2. \tag{10}$$

In the limit of $N \to \infty$, the fraction $(N-1)/N$ tends to unity. Defining $f(x,v,t) = f^{(1)}(x,v,t)$ and using (10), the evolutionary equation (6) of the one-particle DF f transforms to the Fokker-Planck equation

$$\frac{\partial f}{\partial t} + v\frac{\partial f}{\partial x} - (\partial_x \Phi * \rho)\,\frac{\partial f}{\partial v} = -\frac{\partial}{\partial v}\left(D[\Delta v] f\right), \tag{11}$$

where $D[\Delta v] = -\beta(v - u_{\rm f})$ is the diffusion coefficient corresponding to steady drift in the phase space. In deriving equation (11), we have ignored the random motions of particles due to thermal fluctuations. This restricts the applications of our results to flows with Péclet number $\gg 1$.

The macroscopic density $\rho(x,t)$ and the streaming velocity $u(x,t)$ of particles are defined as

$$\rho(x,t) = \int_{-\infty}^{+\infty} f(x,v,t)\,{\rm d}v, \quad u(x,t) = \frac{1}{\rho(x,t)}\int_{-\infty}^{+\infty} v\, f(x,v,t)\,{\rm d}v, \tag{12}$$

and the force field due to particle–particle interactions is computed from the convolution integral

$$\partial_x \Phi * \rho = \int \partial_x \Phi(|x-y|)\,\rho(y)\,{\rm d}y. \tag{13}$$

Our simulations of (11) show that the distribution function acquires a spiky nature in the velocity space. Therefore, it is legitimate to work with a monokinetic velocity distribution of the form $f(x,v,t) = \rho(x,t)\delta(v - u(x,t))$. Numerical calculations that support this assumption will be presented in section IV. Taking the zeroth- and first-order moments of (11) gives the continuity and momentum equations of the particle phase as

$$\frac{\partial \rho}{\partial t} + \frac{\partial}{\partial x}(\rho\, u) = 0, \tag{14}$$

$$\frac{\partial u}{\partial t} + u\,\frac{\partial u}{\partial x} = -\beta(u - u_{\rm f}) - \partial_x \Phi * \rho. \tag{15}$$

We assume that the carrier fluid is incompressible. Its dynamics will therefore be governed by the following continuity and momentum equations:

$$\frac{\partial u_{\rm f}}{\partial x} = 0, \tag{16}$$

$$\rho_{\rm f}\left(\frac{\partial u_{\rm f}}{\partial t} + u_{\rm f}\frac{\partial u_{\rm f}}{\partial x}\right) = -\frac{\partial p_{\rm f}}{\partial x} + \mu_{\rm f}\frac{\partial^2 u_{\rm f}}{\partial x^2} + \beta\rho(u - u_{\rm f}), \tag{17}$$

with $\rho_{\rm f}$, $\mu_{\rm f}$ and $p_{\rm f}$ being the density, viscosity and pressure of the carrier fluid, respectively. Equation (16) implies that $u_{\rm f}$ is only a function of t, and it is prescribed at the inlet of the

one-dimensional flow. Therefore, any change in the spatial density and streaming velocity of the particle phase will locally affect $p_{\rm f}$, which can be computed as the only unknown of the momentum equation (17). We remark that this conclusion does not apply to two- or three-dimensional flows because deformations of streamlines in higher dimensions prevents us from solving the continuity equation independently.

III. NUMERICAL METHODS

Equation (11) can be solved using spectral methods [27], particle in cell (PIC) methods [28], Fourier transform of equations in the velocity subspace [29], and time-splitting method in combination with finite element or finite volume methods [30, 31]. In this paper we have used the last method because of its stability in long-time simulations. Our experiments show that spectral methods are faster, but the results diverge over short time scales. We did not choose PIC methods either because they generate numerical noise, which must be avoided in stability analysis.

We perform time-splitting to reduce the Fokker-Planck equation to two one-dimensional advection problems:

$$\frac{\partial f}{\partial t} + v\frac{\partial f}{\partial x} = 0, \tag{18}$$

$$\frac{\partial f}{\partial t} - (\partial_x \Phi * \rho)\,\frac{\partial f}{\partial v} + \frac{\partial}{\partial v}\left[\beta(v-u_{\rm f})f\right] = 0, \tag{19}$$

which can be solved using flux balance method (FBM) in combination with point-wise weighted essentially non-oscillatory (PWENO) interpolation method. FBM guarantees the conservation of mass, and PWENO interpolation avoids spurious oscillations in computing the higher-order derivatives of the DF f. A detailed description of FBM and PWENO algorithms can be found in [30]. The discretized forms of equations (18) and (19) are

$$\frac{\partial f_{1,j}(x,t)}{\partial t} + \frac{\partial}{\partial x}\left[k_{1,j}(x,t)f_{1,j}(x,t)\right] = 0,\ f_{1,j}(x,t) = f(x,v_j,t),\ j = 1,\ldots,N_2, \tag{20}$$

$$\frac{\partial f_{2,i}(v,t)}{\partial t} + \frac{\partial}{\partial v}\left[k_{2,i}(v,t)f_{2,i}(v,t)\right] = 0,\ f_{2,i}(v,t) = f(x_i,v,t),\ i = 1,\ldots,N_1, \tag{21}$$

where we have used uniform grids in both the x- and v-subspaces and

$$k_{1,j}(x,t) = v_j,\ k_{2,i}(v,t) = -\left[\partial_x\Phi * \rho\right]_{(x_i,t)} + \beta(v-u_{\rm f}). \tag{22}$$

Having $f(x_i,v_j,t_n)$ at all grid points at the nth time step t_n, f is updated at $t_{n+1} = t_n + \Delta t_n$ after three successive steps that utilize FBM and PWENO algorithms: (i) For $1 \le j \le N_2$,

equation (20) is solved in the (x,t)-space over the half time step $\Delta t_n/2$. (ii) The system of N_1 equations (21) is solved in the (v,t)-space over a full time step Δt_n. (iii) Step (i) is repeated for another half time step $\Delta t_n/2$. This procedure assures a second-order accuracy in the time domain [32].

In our simulations we assume the periodic boundary condition $f(0,v,t) = f(X,v,t)$ in the x-direction with X defining the domain of $x \in [0,X]$. The parameter X is estimated based on the flock length L that we introduce in section IV B and find using steady state analytical solutions. Boundary conditions in the velocity space are based on excluding escape solutions: the number density of particles should vanish for $v \to \pm\infty$. In numerical calculations we cannot reach this very limit, and therefore, use a sufficiently large cutoff speed $V > 0$ so that $f(x,v,t) = 0$ for $v \geq +V$ and $v \leq -V$.

To test the convergence of numerical simulations, we start with an initial rectangular $N_1 \times N_2$ mesh $\mathcal{M}_1$ in the (x,v)-space, and compute f and store it at the grid (nodal) points. We then use a second finer mesh $\mathcal{M}_2$ of the size $2N_1 \times 2N_2$, compute f at the grid points of $\mathcal{M}_1$ by interpolating the nodal values of f in $\mathcal{M}_2$. Comparing the first and second sets of nodal DFs, yields the distribution of the computational error in the (x,v)-space. According to our numerical experiments, by taking $N_1 \times N_2 = 500 \times 400$ the maximum relative error is within 2 percent, which shows a reasonable convergence of the FBM and PWENO methods.

IV. COLLECTIVE DYNAMICS IN STEADY FLOWS

A. Simulation of the Fokker-Planck equation

Solving equation (11) is simpler when u_f is constant. In such conditions we identify catastrophic and H-stable phases [6, 18] for the collective dynamics of particles. Consider the following transformations: $\tilde{v} = v - u_\mathrm{f}$ and $\xi = x - u_\mathrm{f} t$, and define $f(x(\xi,t), v(\tilde{v}), t) = \tilde{f}(\xi, \tilde{v}, t)$. The kinetic equation (11) thus becomes

$$\frac{\partial \tilde{f}}{\partial t} + \tilde{v}\frac{\partial \tilde{f}}{\partial \xi} - (\partial_\xi \Phi * \rho)\frac{\partial \tilde{f}}{\partial \tilde{v}} = -\frac{\partial}{\partial \tilde{v}}\left(\beta \tilde{v} \tilde{f}\right), \tag{23}$$

which means the solutions of the Fokker-Planck equation in coordinate frames moving with the constant speed u_f can always be mapped to solutions in stationary frames. Therefore,

if we find a solution $f(x, v, t)$ for $u_{\rm f} = 0$, the function $\tilde{f}(\tilde{x}, \tilde{v}, t) = f(\tilde{x} - u_{\rm f}t, \tilde{v} - u_{\rm f}, t)$ will be a solution of (11) in the $(\tilde{x}, \tilde{v}, t)$ space for any $u_{\rm f} \neq 0$.

For long-range attractions and short-range repulsions, we define new parameters $C = c_1/c_2 > 1$ and $\Delta = d_1/d_2 < 1$, use the initial distribution function

$$f_0(x, v) = f(x, v, 0) = \begin{cases} 10\, e^{-20|v|} & ,\ X/4 < x < 3X/4, \\ 0 & ,\ x < X/4 \text{ or } x > 3X/4, \end{cases} \tag{24}$$

and solve equation (11) using the procedures of section III. Figure 1 shows the snapshots of $f(x, v, t)$ at four different times. At $t = 8$, the DF f very well approximates the steady catastrophic phase with $C\Delta < 1$ and $X = 2$. It is seen that the distribution function eventually takes a spiky form (resembling the Dirac delta function) in the velocity subspace, and all particles move with the same velocity of the carrier fluid. We have observed the spiky nature of the DF for H-stable phase as well. These results justify the assumption of monokinetic DFs used in the derivation of hydrodynamic equations. Figure 2(a) demonstrates the spatial density $\rho(x, t)$ at three different times. The steady state density profile is the one seen at $t = 15$. The pattern of f in the x-subspace depends on C and Δ. The drag coefficient β and $f_0(x, v)$ control the pattern and speed of intermediary stages, and not the final state. For $C\Delta > 1$, the initial DF evolves to an H-stable phase (see Figure 2(b)) whose density profile spreads in the x-domain while the average velocity of particles tends to fluid velocity.

In two dimensional studies the curve $C\Delta^2 = 1$ is the separatrix (in the parameter space) between H-stable and catastrophic phases [6], but in one dimensional systems the separatrix is the curve $C\Delta = 1$ [18], which is in agreement with our results. The final stable density pattern in the catastrophic phase correlates with the value of $C\Delta$ (Figure 2(c)). It is evident that increasing $C\Delta$ yields larger stable flock lengths.

B. Analytical solutions for steady flocks

The final state of f in Figure 1 suggests that we can find an exact solution for $\rho(x, t)$ in catastrophic conditions. Since particles eventually acquire the same velocity of the carrier fluid, one can start with the monokinetic DF $f(x, v, t) = \rho(x, t)\delta(v - u(x, t))$ and the traveling density pattern $\rho(x, t) = \rho(x - u_{\rm f}t)$ where $u(x, t) = u_{\rm f}$. Substituting these assumptions into

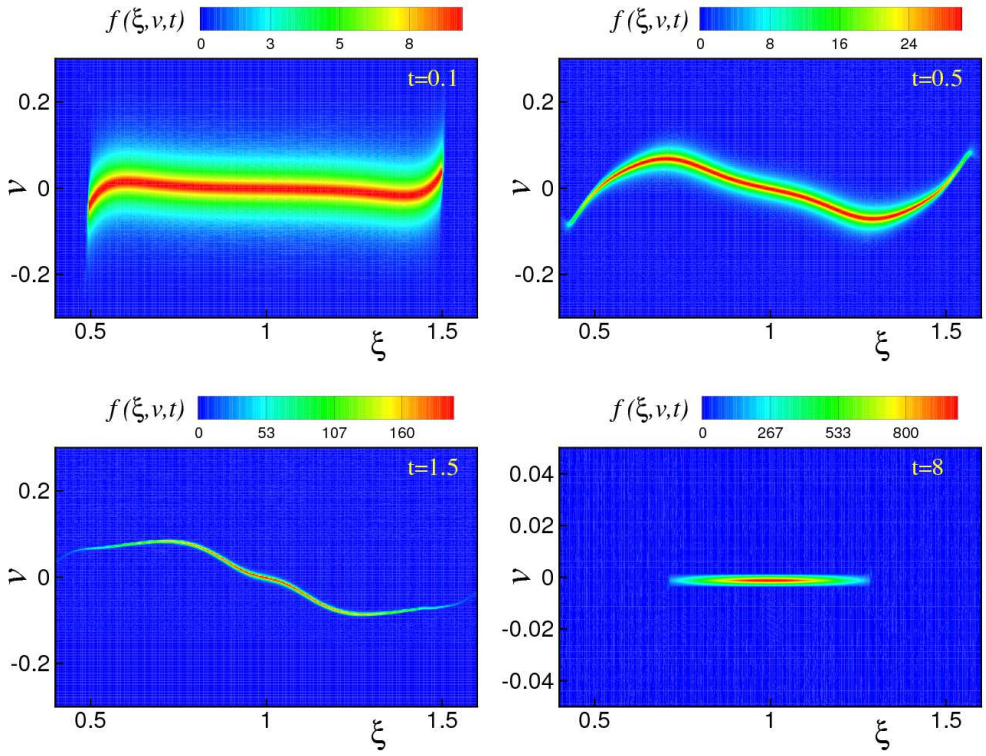

FIG. 1. Evolution of distribution function $f(\xi, v, t)$ with $\xi = x - u_{\rm f}t$ in a catastrophic phase. The initial state of the system is given by equation (24) where $X = 2$. The parameters of the potential Φ are set to $c_1 = 1.5$, $c_2 = 1.0$, $d_1 = 0.05$ and $d_2 = 0.1$. Snapshots correspond to $t = 0.1$, 0.5, 1.5, and 8. Note the scale of v-axis in the bottom-right panel. The distribution function eventually converges to $f(\xi, v, t) = \rho(\xi)\delta(v - u_{\rm f})$.

the hydrodynamic equations (14) and (15), and using the co-moving coordinate $\xi = x - u_{\rm f}t$, we obtain the integral equation

$$\partial_\xi \Phi * \rho = \frac{c_1}{d_1}(\mathcal{B}_1 - \mathcal{A}_1) + \frac{c_2}{d_2}(\mathcal{A}_2 - \mathcal{B}_2) = 0, \tag{25}$$

where

$$\mathcal{A}_i(\xi) = \int_0^\xi e^{-\frac{1}{d_i}(\xi-\eta)}\rho(\eta)\,\mathrm{d}\eta, \quad \mathcal{B}_i(\xi) = \int_\xi^L e^{\frac{1}{d_i}(\xi-\eta)}\rho(\eta)\,\mathrm{d}\eta, \quad i = 1, 2, \tag{26}$$

and L is a to-be-determined flock length. Differentiating equation (25) four times with respect to ξ, and eliminating $\mathcal{A}_i$ and $\mathcal{B}_i$ $(i = 1, 2)$ from calculations, lead to

$$\frac{\partial^3 \rho}{\partial \xi^3} - \frac{C\Delta - 1}{d_1 d_2 (C - \Delta)}\frac{\partial \rho}{\partial \xi} = 0, \tag{27}$$

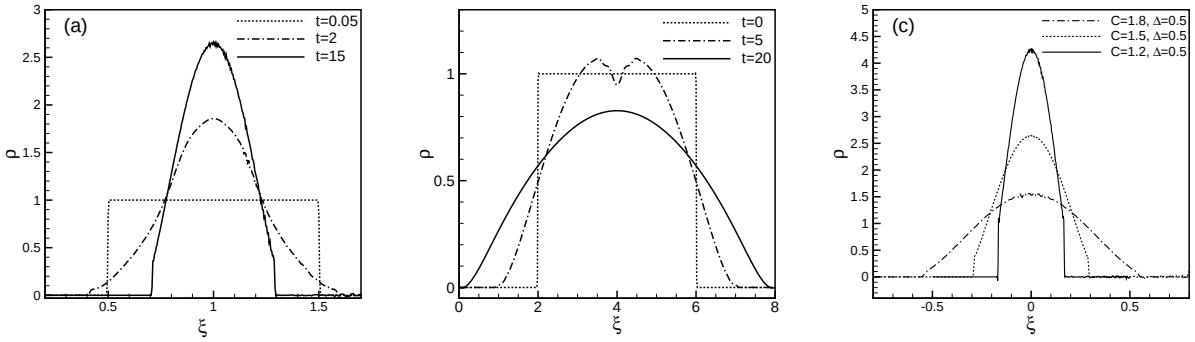

FIG. 2. (a) Evolution of spatial density ρ obtained from the simulations of the Fokker-Planck equation in catastrophic phase for $\beta = 2$, $c_1 = 1.5$, $c_2 = 1$, $d_1 = 0.05$, and $d_2 = 0.1$. The initial DF has been computed from equation (24) with $X = 2$. (b) Evolution of ρ in H-stable phase for a model with $\beta = 0.5$, $c_1 = 2.2$, $c_2 = 1$, $d_1 = 0.05$, and $d_2 = 0.1$. The density profile spreads to a finally flat state. The initial distribution is similar to equation (24) but with $X = 8$. (c) Relaxed stable density profiles for three models in the catastrophic phase. In all cases we have used $\beta = 0.5$, $c_2 = 1$, $d_1 = 0.05$, and $d_2 = 0.1$. It is evident that the flock length increases proportional to C.

whose solution is

$$\rho = b_0 + b_1 e^{\alpha_1 \xi} + b_2 e^{\alpha_2 \xi}, \quad \alpha_1 = +\sqrt{\frac{C\Delta - 1}{d_1 d_2 (C - \Delta)}}, \quad \alpha_2 = -\sqrt{\frac{C\Delta - 1}{d_1 d_2 (C - \Delta)}}, \tag{28}$$

Due to long-range attraction and short-range repulsion we always have $C > \Delta$. Therefore, α_i $(i = 1, 2)$ will be real numbers if $C\Delta > 1$, and pure imaginary numbers otherwise. We substitute from (28) into equation (25) and its first derivative with respect to ξ, then evaluate the four resulting equations at $\xi = 0$ and $\xi = L$ to obtain

$$\begin{bmatrix} B_{11} & B_{12} & B_{13} \\ B_{21} & B_{22} & B_{23} \\ B_{11} & e^{\alpha_1 L} B_{13} & e^{\alpha_2 L} B_{12} \\ B_{21} & e^{\alpha_1 L} B_{23} & e^{\alpha_2 L} B_{22} \end{bmatrix} \cdot \begin{Bmatrix} b_0 \\ b_1 \\ b_2 \end{Bmatrix} = \mathbf{0}, \tag{29}$$

where

$$B_{i1} = d_i, \quad B_{i2} = \frac{C^{i-2}(1 - \alpha_1 d_i)(C - \Delta)}{d_2(1 - \Delta^2)}, \quad B_{i3} = \frac{C^{i-2}(1 - \alpha_2 d_i)(C - \Delta)}{d_2(1 - \Delta^2)}, \tag{30}$$

and $i = 1, 2$. Non-trivial solutions exist for b_0, b_1 and b_2 should the determinants of all 3×3 sub-matrixes in the coefficient matrix of equation (29) vanish. This gives the unique

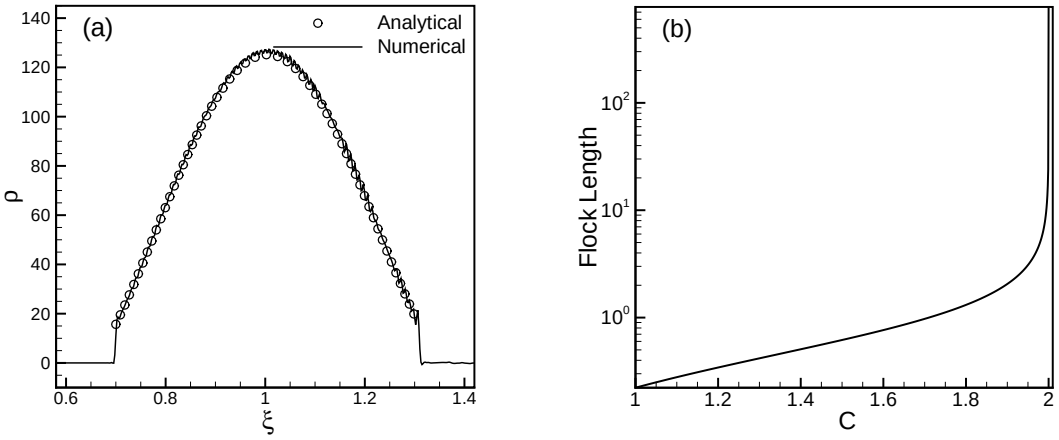

FIG. 3. (a) Relaxed density ρ in a catastrophic phase computed using the Fokker-Planck equation (solid line) and analytical results of section IV B (circles). Model parameters are $d_1 = 0.1$, $d_2 = 0.05$, $c_1 = 1.5$, and $c_2 = 1$. (b) Variation of the flock length L in terms of C for a model with $d_1 = 0.05$, $d_2 = 0.1$ and $C_2 = 1$.

solution:

$$e^{\alpha_1 L} = \frac{C(1-\Delta)[d_1\alpha_1(C-\Delta)+1-C\Delta]}{d_1\alpha_1(C-\Delta)(C\Delta+C-2)+(C\Delta-1)(C\Delta+C-2\Delta)}, \tag{31}$$

from which one finds L. Equation (28) shows that α_1 has a real positive value for H-stable solutions with $C\Delta > 1$. By substituting for α_1 from (28) into (31), and imposing $C\Delta > 1$, $C > 1$ and $\Delta < 1$, one can verify that $e^{\alpha_1 L} < 1$. This corresponds to a non-physical flock length $L < 0$ as is expected: the H-stable phase does not admit any characteristic/flock length. In the catastrophic phase with a pure imaginary α_1, the right hand side of equation (31) becomes a complex number as $\exp[\mathrm{i}\,\gamma(C,\Delta)]$ with $\mathrm{i} = \sqrt{-1}$ and $0 \le \gamma \le 2\pi$. Our calculations show that the physical flock length corresponding to $\rho(\xi) \ge 0$ becomes $L = \mathrm{i}\gamma/\alpha_1$. Once L is computed, the constant coefficients b_0, b_1 and b_2 can be calculated from (29).

Figure 3(a) compares $\rho(\xi)$ profiles obtained from (28) and numerical solutions of the Fokker-Planck equation. There is an impressive match between the two sets of results, providing a bench mark for our more complex computations in section V A. In Figure 3(b) we have plotted L versus the parameter C for $\Delta = 0.5$. It is seen that the flock length tends to infinity as $C\Delta \to 1$. This is because $\alpha_1 \to 0^+ i$, which indicates the transition boundary from the catastrophic to H-stable phase. For $C\Delta = 1$, equation (27) transforms

to $\partial^3\rho/\partial\xi^3 = 0$ whose solution is $\rho = b_0 + b_1\xi + b_2\xi^2$. Employing the boundary conditions at $\xi = 0$ and $\xi = L$, one obtains a system of determinantal equations that have no root for finite values of $L > 0$. We thus conclude that the boundary line $C\Delta = 1$ in the parameter space belongs to the H-stable phase with no characteristic/flock length.

V. COLLECTIVE DYNAMICS IN UNSTEADY FLOWS

We now consider time-varying $u_{\rm f}(t)$, search for base-state solutions in the catastrophic phase, and investigate their stability. We think of a co-moving coordinate system with the velocity $u_\beta(t)$, and carry out the following change of spatial variable:

$$\xi = x - \int_0^t u_\beta(\tau)\, d\tau. \tag{32}$$

The velocity $u_\beta(t)$ is yet to be determined with the aim of eliminating explicit time-dependent terms from the continuity and momentum equations. In the co-moving frame, the density and streaming velocity of particles are expressed as $\tilde\rho(\xi,t) = \rho(x(\xi,t),t)$ and $\tilde u(\xi,t) = u(x(\xi,t),t)$, respectively. Equations (14) are thus transformed to

$$\frac{\partial\tilde\rho}{\partial t} + (\tilde u - u_\beta)\frac{\partial\tilde\rho}{\partial\xi} + \tilde\rho\frac{\partial\tilde u}{\partial\xi} = 0, \tag{33}$$

$$\frac{\partial\tilde u}{\partial t} + (\tilde u - u_\beta)\frac{\partial\tilde u}{\partial\xi} + \beta[\tilde u - u_{\rm f}(t)] + \partial_\xi\Phi * \tilde\rho = 0, \tag{34}$$

which explicitly depend on t through the terms involving $u_\beta(t)$ and $u_{\rm f}(t)$. These terms are eliminated should u_β be the particular solution of the following ordinary differential equation

$$\frac{{\rm d}u_\beta}{{\rm d}t} + \beta[u_\beta(t) - u_{\rm f}(t)] = 0. \tag{35}$$

Consequently, equations (33) and (34) become

$$\partial\tilde\rho_0/\partial t = 0, \quad \tilde u_0 = u_\beta, \quad \partial_\xi\Phi * \tilde\rho_0 = 0, \tag{36}$$

where $\tilde\rho_0$ and $\tilde u_0$ are *traveling wave solutions*. Therefore, while the invariant shape of the spatial density profile given in equation (28) travels according to (32), the streaming velocity of particles varies over time but it is not identical to $u_{\rm f}(t)$. Using (35), one can determine the effect of amplitude and frequency of a pulsating carrier fluid (similar to blood flow) on particle streaming. For instance, a periodic excitation $u_{\rm f} = A_0 + A_1\sin(\Omega t)$ yields

$$\tilde u = A_0 + \frac{\beta^2\, A_1}{(\Omega^2+\beta^2)}\sin(\Omega t) - \frac{\Omega\beta\, A_1}{(\Omega^2+\beta^2)}\cos(\Omega t). \tag{37}$$

This shows that increasing the pulse frequency suppresses the periodic nature of particle streaming: for $\Omega \gg 1$ particles will not follow the carrier fluid, unless $\beta \to \infty$. Our numerical simulations confirm this effect.

A. Stability of unsteady flocks

An important question is whether the collective flock of particles is stable under time-varying fluid velocities. To answer this question, we perturb macroscopic quantities as $\tilde{u} = \tilde{u}_0(t) + \tilde{u}_1(\xi, t)$ and $\tilde{\rho} = \tilde{\rho}_0(\xi) + \tilde{\rho}_1(\xi, t)$, and linearize equations (33) and (34) to obtain

$$\frac{\partial \tilde{\rho}_1}{\partial t} + \frac{\partial}{\partial \xi}\left(\tilde{u}_1 \tilde{\rho}_0\right) = 0, \quad \frac{\partial \tilde{u}_1}{\partial t} + \beta \tilde{u}_1 + \partial_\xi \Phi * \tilde{\rho}_1 = 0. \tag{38}$$

These equations can be solved through a Fourier transformation in the time domain followed by an expansion in terms of suitable basis functions in the ξ-space. Nevertheless, equations (38) are linear and solutions in the Fourier transform space will be decoupled for different frequencies. We can thus assume $\tilde{u}_1 = U(\xi)e^{\Omega t}$ and $\tilde{\rho}_1 = R(\xi)e^{\Omega t}$, substitute them in (38) and eliminate $R(\xi)$ between the linearized continuity and momentum equations. This leaves us with the eigenvalue problem

$$\int_0^L \partial_\xi \Phi(|\xi - \eta|) \frac{\partial}{\partial \eta}\left[U(\eta)\tilde{\rho}_0(\eta)\right] d\eta = \lambda U(\xi), \quad \lambda = -\Omega(\Omega + \beta), \tag{39}$$

whose solutions can then be superposed in the λ-space (using a discrete summation or a continuous integral, whichever applies) to obtain the most general expressions for $\tilde{u}_1$ and $\tilde{\rho}_1$. Integrating (39) by parts gives

$$\begin{aligned}\left[2\partial_\xi \Phi(0^+)\,\tilde{\rho}_0(\xi) + \lambda\right] U(\xi) + \partial_\xi \Phi(|\xi - L|)\,\tilde{\rho}_0(L)U(L) - \partial_\xi \Phi(\xi)\,\tilde{\rho}_0(0)U(0) \\ + \int_0^L K(\xi, \eta)\, U(\eta)\, \mathrm{d}\eta = 0,\end{aligned} \tag{40}$$

which is a Fredholm-type integral equation with the kernel $K(\xi, \eta) = \tilde{\rho}_0(\eta)\partial_{\xi\xi}\Phi(|\xi - \eta|)$. We could not find a complete set of basis functions to expand $U(\xi)$, and adopted an implicit numerical method to solve (40) and compute the eigenvalue λ. We divide the ξ-space to N equally spaced intervals with the increments $\Delta\xi = L/N$, and take $U_j = U(j\Delta\xi)$ $(j = 0, 1, \ldots, N)$ as unknown variables. The definite integral involving the kernel is then computed using the trapezoidal rule and equation (40) is transformed to the linear eigensystem $\mathbf{A} \cdot \boldsymbol{U} = \lambda \boldsymbol{U}$ where $\mathbf{A}$ is a constant matrix and $\boldsymbol{U}$ is a column vector assembled from U_j. The eigenvalue problem is solved using standard LAPACK libraries.

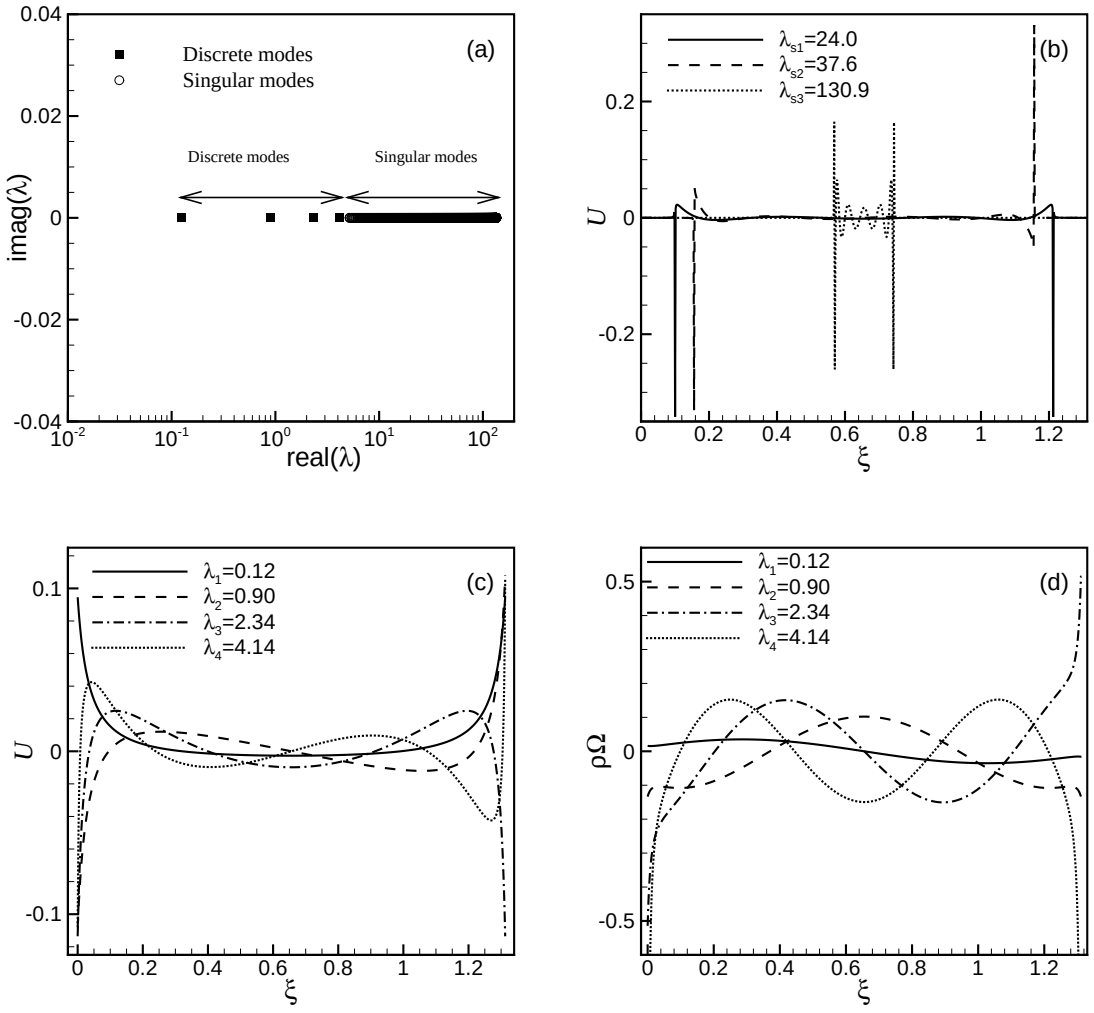

FIG. 4. (a) Eigenvalue spectrum of linearized equations (38) in the vicinity of a time-varying $u_{\rm f}(t)$ for a model with $c_1 = 3.6$, $c_2 = 2$, $d_1 = 0.05$, and $d_2 = 0.1$. Equations (38) are normalized with respect to the total number of particles so that $\int_0^L \rho_0(\xi)\,{\rm d}\xi = 1$. Discrete global modes are shown with filled squares. Singular modes (circles) form a continuous family. Discrete modes converge within 0.5% relative error by taking $N > 400$ where N is the number of discrete grid points in the ξ-space. Increasing N adds new singular modes to the continuous part of the spectrum. (b) Patterns of three singular modes for $\lambda_{s1} = 24.0$, $\lambda_{s2} = 37.6$ and $\lambda_{s3} = 130.9$. One can verify that the locations of spikes are consistent with the roots of equation (41). (c) Perturbed velocity patterns of all discrete global modes. (d) Perturbed density patterns of all global modes.

Interestingly, we find that the eigenspectrum contains a continuous spectrum of singular modes and a finite number of discrete global modes as shown in Figure 4(a). Singular modes emerge when the coefficient of $U(\xi)$ in the first term of (40) vanishes at $\xi_s \in [0, L]$ so that

$$\lambda_s = -2\partial_\xi \Phi(0^+)\, \tilde{\rho}_0(\xi_s). \tag{41}$$

In the Catastrophic phase, $\tilde{\rho}_0$ is a single-peaked function and equation (41) is satisfied at two points, ξ_{s1} and ξ_{s2}. The mode shape $U(\lambda_s, \xi)$ corresponding to λ_s thus becomes spiky at $\xi = \xi_{s1}$ and $\xi = \xi_{s2}$, and manages to annul the definite integral in (40). Singular modes have zero amplitudes at the boundaries, so that $U(\lambda_s, 0) = U(\lambda_s, L) = 0$, unless for the eigenvalue associated with $\xi_{s1} = 0$ and $\xi_{s2} = L$. Figure 4(b) demonstrates the shapes of three singular modes. Discrete global modes have been shown in Figure 4(c). It is evident that they are smooth and the number of their nodes increases proportional to λ. All eigenvalues that we find are positive real numbers and the mode frequencies are computed as $\Omega_{1,2} = -\beta/2 \pm \sqrt{\beta^2/4 - \lambda}$, which always has a negative real part. The traveling catastrophic solutions are therefore stable. Discrete modes will generate global, long-lived oscillatory patterns if $\beta \ll 1$ and $\beta^2 < 4\lambda$. A mode will be overdamped and critically damped for $\beta^2 > 4\lambda$ and $\beta^2 = 4\lambda$, respectively. Our computations show that λ decreases by increasing C and Δ. For each eigenmode $U(\lambda, \xi)$ we obtain two *eigendensities*:

$$R_i(\lambda, \xi) = -\frac{1}{\Omega_i} \frac{\partial}{\partial \xi} \left[\tilde{\rho}_0(\xi) U(\lambda, \xi)\right], \quad i = 1, 2. \tag{42}$$

Therefore, any perturbed state will be represented as a linear combination

$$(\tilde{\rho}_1, \tilde{u}_1) = (a_1 \tilde{\rho}_{11} + a_2 \tilde{\rho}_{12}, a_1 \tilde{u}_{11} + a_2 \tilde{u}_{12}), \tag{43}$$

where a_1 and a_2 are constant coefficients and

$$(\tilde{\rho}_{1j}, \tilde{u}_{1j}) = [R_j(\lambda, \xi), U(\lambda, \xi)]\, e^{\Omega_j t}. \tag{44}$$

To this end, we show that a linearly stable mode of the perturbed continuity and momentum equations is also a stable solution of the full nonlinear Fokker-Planck equation. We set $a_1 = -a_2 = 0.5\Omega_1\Omega_2/(\Omega_2 - \Omega_1)$ and start from the initial DF

$$f(x, v, 0) = \left[\tilde{\rho}_0 + a_1 \left(\tilde{\rho}_{11} - \tilde{\rho}_{12}\right)\right] \delta(v), \tag{45}$$

to numerically solve equation (11) and trace the transient dynamics of the second discrete mode (with $\lambda_2 = 0.90$) in the model of Figure 4. In the linear regime, this mode decays

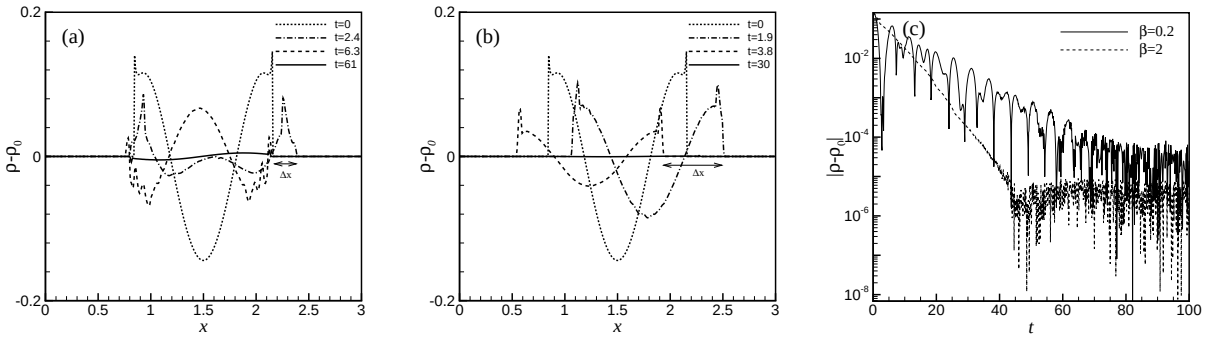

FIG. 5. Evolution of $\rho_1(x,t)$ obtained through solving the Fokker-Planck equation. The initial DF is computed from equation (43). Panels (a) and (b) correspond to $\beta = 0.2$ and $\beta = 2$, respectively. Δx shows the travel range of the flock as the carrier fluid velocity varies according to $u_{\rm f}(t) = 0.3\cos(\omega t)$. Panel (c) illustrates the variation of $|\rho_1(x,t)|$ at $\xi = L/2$.

monotonically for $\beta \geq 1.89$ and becomes an underdamped oscillatory wave otherwise. Figure 5 shows several snapshots of $\rho_1(x,t) = \rho(x,t) - \rho_0(x,t)$ for $\beta = 0.2$ and $\beta = 2.0$ where $\rho_0(x,t) = \tilde{\rho}_0(\xi(x,t))$ is the traveling base-state density of particles. We have set the velocity of the carrier fluid to $u_{\rm f}(t) = 0.3\cos(\omega t)$ with $\omega = 0.94$, which is equal to $\mathrm{Im}(\Omega_{1,2})$ when $\lambda_2 = 0.90$ and $\beta = 0.2$. Figure 5(a) demonstrates that the traveling perturbation is damped while it oscillates. No oscillation is seen in Figure 5(b) for $\beta = 2$ as is expected. Although the flock velocity is asynchronous with $u_{\rm f}(t)$, the particle density has ultimately acquired its invariant traveling form $\tilde{\rho}_0(\xi)$. This is in agreement with our analytical results. In Figure 5, Δx indicates the travel range of the entire flock as it responds to the pulsed flow. Our results show that after four oscillation cycles of $u_{\rm f}(t)$, $|\rho_1(x,t)|$ drops to 3.4% and 0.1% of its initial value for $\beta = 0.2$ and $\beta = 2$, respectively. Figure 5(c) shows the temporal variation of $|\rho_1(x,t)|$ at $\xi = L/2$. The oscillatory behavior for $\beta = 0.2$, and overdamped response for $\beta = 2$ are evident in Figure 5(c). In both cases the envelope (or wave amplitude) decays linearly in the logarithmic scale, except in regions dominated by numerical noise as $|\rho_1(x,t)| \to 0$.

VI. CONCLUSIONS

We studied the collective dynamics of interacting particles in steady and unsteady one-dimensional flows. One dimensional swarms of particles can be observed in microchannels when the sizes of particles and channel cross section are comparable. For instance, the collective motion of RBCs in micro vessels is a one-dimensional problem, especially when RBCs take a parachute shape [33]. Track cycling is another prominent one-dimensional problem where the members of a team collaborate along their path to minimize the drag force. Particle–particle interaction was modeled using the Morse potential. It was assumed that the carrier fluid is not disturbed by the particle phase although particles communicate with the carrier fluid through drag force. The evolution of the phase space distribution function of particles towards H-stable and catastrophic phases was investigated by keeping inertial effects. These phases had been studied previously [18, 21, 22], but in the absence of acceleration terms in momentum equations.

One of the fundamental results of this study is the existence of two general families of discrete and singular decaying modes, which are calculated from a Fredholm-type eigenvalue problem. Singular modes are local disturbances supported by interactions of immediate neighbors, i.e., the information of local changes in the particle density is not communicated with the entire flock. Singular modes found here can be represented as the weighted sums of Dirac's delat functions, and they are analogous to van Kampen modes [34] in plasma oscillations. They are expected to form a complete set and be superposed to reconstruct a wide variety of density waves. Discrete modes, however, globally influence the flock and can be regarded as secondary collective effects developed in the vicinity of $\tilde{\rho}_0(\xi)$. It is noted that singular modes are the characteristics of systems of interacting particles and they *do not exist* in fluids.

Our findings have interesting implications for the flock of birds and fishes whose skins and body shapes have evolved to minimize drag force: in low-drag limits, discrete modes and superpositions of singular modes appear as long-lived, oscillatory density waves that travel through the entire population without disintegrating the flock. The only prerequisite for such a behavior is initially being in the catastrophic phase. Therefore, the collective flock of birds and fishes can exhibit a rich set of stable time-varying patterns, which should be observable during their group motions.

Whether discrete and singular modes exist in two- and three-dimensional systems is an open problem. The difficulty of higher dimensional systems is to analyze the deformations of contact lines/surfaces between the particle and fluid phases (this problem does not exist in one-dimensional flows). In two dimensional systems a rotating vortex can emerge as the steady state solution [6, 22]. An interesting unsolved problem is to understand the linear stability of vortices. For doing so, one can adopt the usual polar coordinates (R, ϕ) to describe the governing equations. It is then possible to represent azimuthal perturbations using the Fourier series of ϕ, and formulate the eigenvalue problem in terms of unknown functions that describe the radial variations of the particle density and two streaming velocity components. Singular two-dimensional modes may be produced from exact resonances between the radial and azimuthal motions of particles. Discrete modes, regardless of their stable or unstable nature, are also possible in the form of traveling spiral waves, analogous to density waves in self-gravitating stellar systems whose dynamics is represented by the collisionless Boltzmann equation [35].

ACKNOWLEDGMENTS

We thank anonymous referees for their useful comments, which helped us to substantially improve the presentation of the paper.

[1] D. S. Cambui, and A. Rosas, *Density induced transition in a school of fish*, Physica A: Statistical Mechanics and its Applications, 391 (2012), pp. 3908-3914.

[2] I. Daruka, *A phenomenological model for the collective landing of bird flocks*, Proc. R. Soc. B, 276 (2009), pp. 911-917.

[3] K. Boryczko, W. Dzwinel, and D. A. Yuen, *Dynamical clustering of red blood cells in capillary vessels*, J. Mol. Model., 9 (2003), pp. 16-33.

[4] X. Chen, X. Dong, A. Be'er, H. L. Swinney, and H. P. Zhang, *Scale-invariant correlations in dynamic bacterial clusters*, Phys. Rev. Lett., 108 (2012), paper 148101.

[5] T. Vicsek, A. Czirok, E. Ben-Jacob, F. I. Cohen, and O. Shochet,*Novel type of phase transition in a system of self-driven particles*, Phys. Rev. Lett., 75 (1995), pp. 1226-1229.

[6] M. R. D'Orsogna, Y. L. Chuang, A. L. Bertozzi, and L. S. Chayes, *Self-propelled particles with soft-core interactions: patterns, stability, and collapse*, Phys. Rev. Lett., 96 (2006), paper 104302.

[7] S.-Y. Ha, and E. Tadmor, *From particle to kinetic and hydrodynamic descriptions of flocking*, Kinetic and Related Models, 1 (2008), pp. 415-435.

[8] M. Fornasier, J. Haskovec, and G. Toscani, *Fluid dynamic description of flocking via the PovznerBoltzmann equation*, Physica D: Nonlinear Phenomena, 240 (2011), pp. 21-31.

[9] M. Agueh, R. Illner, and A. Richardson, *Analysis and simulations of a refined flocking and swarming model of Cucker-Smale type*, Kinetic and Related Models, 4 (2011), pp. 1-16.

[10] J. Shen 2008, *CuckerSmale Flocking under Hierarchical Leadership*, SIAM J. Appl. Math., 68 (2008), pp. 694-719.

[11] G. Baglietto, and E. V. Albano, *Nature of the order-disorder transition in the Vicsek model for the collective motion of self-propelled particles*, Phys. Rev. E, 80 (2009), paper 050103.

[12] A. Babloyantz, and A. Destexhe, *Is the normal heart a periodic oscillator?*, Biological Cybernetics, 58 (1988) pp. 203-211.

[13] F. Peters, C. Marrasé, H. Havskum, F. Rassoulzadegan, J. Dolan, M. Alcaraz, and J. M. Gasol, *Turbulence and the microbial food web: effects on bacterial losses to predation and on community structure*, J. Plankton Res., 24 (2002), pp. 321-331.

[14] R. S. Marcos, *Microorganisms in vortices: a microfluidic setup*, Limnol. Oceanogr. Methods, 4 (2006), pp. 392-398.

[15] W. M. Durham, J. O. Kessler, and R. Stocker, *Disruption of vertical motility by shear triggers formation of thin phytoplankton layers*, Science, 323 (2009), pp. 1067-1070.

[16] A. Chertock, K. Fellner, A. Kurganov, A. Lorz, and P. A. Markowich, *Sinking, merging and stationary plumes in a coupled chemotaxisuid model: a high-resolution numerical approach*, J. Fluid Mech., 694 (2012), pp. 155-190.

[17] T. J. Pedley, and J. O. Kessler, *Hydrodynamic phenomena in suspensions of swimming microorganisms*, Annu. Rev. Fluid Mech., 24 (1992), pp. 313-358.

[18] A. J. Leverentz, C. M. Topaz, and A. J. Bernoff, *Asymptotic dynamics of attractive-repulsive swarms*, SIAM J. Appl. Dyn. Syst., 8 (2009), pp. 880-908.

[19] J. H. von Brecht, D. Uminsky, T. Kolokolnikov, and A. L. Bertozzi, *Predicting*

pattern formation in particle interactions, Math. Models Methods Appl. Sci., 22 (2012), paper 1140002.

[20] E. J. Hackett-Jones, K. A. Landman, and K. Fellner, *Aggregation patterns from nonlocal interactions: discrete stochastic and continuum modeling*, Phys. Rev. E, 85 (2012), paper 041912.

[21] A. J. Bernoff, and C. M. Topaz, *A primer of swarm equilibria*, SIAM J. Appl. Dyn. Syst., 10 (2011), pp. 212-250.

[22] H. Levine, W. J. Rappel, and I. Cohen, *Self-organization in systems of self-propelled particles*, Phys. Rev. E., 63 (2001), paper 017101.

[23] D. Ruelle, *Statistical Mechanics, Rigorous Results* (W. A. Benjamin, Inc., New York, 1969).

[24] Y. Liu, and W. K. Liu, *Rheology of red blood cell aggregation by computer simulation*, Journal of Computational Physics, 220 (2006), pp. 139-154.

[25] C. M. Topaz, A. J. Bernoff, S. Logan, and W. Toolson, *A model for rolling swarms of locusts*, The European Physical Journal Special Topics, 157 (2008), pp. 93-109

[26] J. A. Carrillo, M. R. D'Orsogna, and V. Panferov, *Double milling in self-propelled swarms from kinetic theory*, Kinetic and Related Models, 2 (2009), pp. 363-378.

[27] L. Gibelli, and B. D. Shizgal, *Short note: Spectral convergence of the Hermite basis function solution of the Vlasov equation: the free-streaming term*, Journal of Computational Physics, 219 (2006), pp. 477-488.

[28] G. B. Jacobs, and J. S. Hesthaven, *High-order nodal discontinuous Galerkin particle-in-cell method on unstructured grids*, Journal of Computational Physics, 214 (2006), pp. 96-121.

[29] B. Eliasson, *Numerical Simulations of the Fourier-Transformed Vlasov-Maxwell System in Higher Dimensionstheory and Applications*, Transport theory and Statistical Physics, 39 (2011), pp. 387-465.

[30] J. A. Carrillo, and F. Vecil, *Nonoscillatory interpolation methods applied to Vlasov-based models*, SIAM J. Sci. Comput., 29 (2007), pp. 1179-1206.

[31] J. M. Qiu, and A. Christlieb, *A conservative high order semi-Lagrangian WENO method for the Vlasov equation*, Journal of Computational Physics, 229 (2010), pp. 1130-1149.

[32] C. Z. Cheng and G. Knorr, *The Integration of the Vlasov Equation in Configuration Space*, Journal of Computational Physics, 22 (1976), pp. 330-351.

[33] J. L. McWhirter, H. Noguchi, and G. Gompper, *Flow-induced clustering and alignment*

of vesicles and red blood cells in microcapillaries, Proceedings of the National Academy of Sciences of the United States of America, 106 (2009), pp. 6039-6043.

[34] N. G. van Kampen, *On the theory of stationary waves in plasmas*, Physica, 21 (1955), pp. 949-963.

[35] M. A. Jalali, *Unstable disk galaxies. I. Modal properties*, The Astrophysical Journal, 669 (2007), pp. 218-231.